Chemical biofilm removal capacity of endodontic irrigants as a function of biofilm structure

Busanello, F; Petridis, X; So, M V R; Dijkstra, R J B; Sharma, P K; van der Sluis, L W M

Published in:
International Endodontic Journal

DOI:
10.1111/iej.13027

INTERNATIONAL
ENDODONTIC JOURNAL

doi:10.1111/iej.13027

Chemical biofilm removal capacity of endodontic irrigants as a function of biofilm structure: optical coherence tomography, confocal microscopy and viscoelasticity determination as integrated assessment tools

F. H. Busanello[1,†], X. Petridis[2,†], M. V. R. So[1], R. J. B. Dijkstra[2], P. K. Sharma[3] & L. W. M. van der Sluis[2]

[1]Conservative Dentistry Department, School of Dentistry, Federal University of Rio Grande do Sul, Porto Alegre, Rio Grande do Sul, Brazil; [2]Department of Conservative Dentistry, Center for Dentistry and Oral Hygiene; and [3]Department of Biomedical Engineering, University Medical Center Groningen, University of Groningen, Groningen, The Netherlands

Abstract

Busanello FH, Petridis X, So MVR, Dijkstra RJB, Sharma PK, van der Sluis LWM. Chemical biofilm removal capacity of endodontic irrigants as a function of biofilm structure: optical coherence tomography, confocal microscopy and viscoelasticity determination as integrated assessment tools. *International Endodontic Journal*, **52**, 461–474, 2019.

Aim To investigate the influence of biofilm structure on the biofilm removal capacity of endodontic irrigants and to study changes in the architecture of the remaining biofilms.

Methodology *Streptococcus oralis* J22 and *Actinomyces naeslundii* T14V-J1 were cocultured under different growth conditions on saliva-coated hydroxyapatite discs. A constant depth film fermenter (CDFF) was used to grow steady-state 4-day biofilms. Biofilms were grown under static conditions for 4 and 10 days within a confined space. Twenty microlitres of 2% NaOCl, 2% Chlorhexidine (CHX), 17% Ethylene-diamine-tetra-acetic acid (EDTA) and buffer were applied statically on the biofilms for 60 s. Biofilm removal was evaluated with optical coherence tomography (OCT). Post-treated biofilms were assessed via low load compression testing (LLCT) and Confocal laser scanning microscopy (CLSM). Optical coherence tomography data were analysed through a two-way analysis of variance (ANOVA). Low load compression testing and CLSM data were analysed through one-way ANOVA and Dunnett's *post hoc* test. The level of significance was set at $a < 0.05$.

Results The initial biofilm structure affected the biofilm removal capacity of the irrigants. NaOCl demonstrated the greatest chemical efficacy against the biofilms and was significantly more effective on the static than the CDFF biofilms ($P < 0.001$). CHX was ineffective and caused a rearrangement of the biofilm structure. Ethylene-diamine-tetra-acetic acid exhibited a distinct removal effect only on the CDFF biofilms. Biofilm age influenced the structure of the remaining biofilms. The 4-day grown remaining biofilms had a significantly different viscoelastic pattern compared to the respective 10-day grown biofilms ($P \leq 0.01$),

Correspondence: Xenos Petridis, Department of Conservative Dentistry, Center for Dentistry and Oral Hygiene, University Medical Center Groningen, University of Groningen, Antonius Deusinglaan 1, 9713 AV, Groningen, The Netherlands (tel.: + 31 6 29464747; e-mails: x.petridis@umcg.nl; xenous7@hotmail.com).

[†]Both authors contributed equally to this study and should both be listed as first authors.

especially in the NaOCl-treated group. Confocal laser scanning microscopy analysis confirmed the CHX-induced biofilm structural rearrangement.

Conclusions Biofilm structure is an influential factor on the chemical efficacy of endodontic irrigants. Optical coherence tomography allows biofilm removal characteristics to be studied. NaOCl should remain the primary irrigant. Ethylene-diamine-tetra-acetic acid was effective against cell-rich/EPS-poor biofilms. Chlorhexidine did not remove biofilm, but rather rearranged its structure.

Keywords: biofilm, irrigants, optical coherence tomography, removal, structure, viscoelasticity.

Received 12 June 2018; accepted 3 October 2018

Introduction

Apical periodontitis is the reaction of the host immune system to micro-organisms mainly located within the root canal system (Nair 2004). Although complete eradication of the microbial infection is the theoretical aim of root canal treatment, this has been considered as an unrealistic task due to the complex intraradicular anatomy and the biofilm mode of microbial colonization (Nair *et al.* 2005, Ricucci & Siqueira 2010). However, lowering the biofilm burden below a threshold that would allow healing to take place seems to be the pragmatic aim of root canal treatment (Siqueira & Rôças 2008). Therefore, from a clinical standpoint, the effect of the most widely employed endodontic irrigants on biofilm removal becomes extremely relevant. In addition, studying the structure of the biofilm that persists after disinfection procedures could aid in developing more effective removal regimes (Ohsumi *et al.* 2015).

Biofilms have a distinct structure comprised mainly of water, a matrix of extracellular polymeric substances (EPS) and the micro-organisms (Flemming & Wingender 2010). This structural organization determines the susceptibility of biofilms to biocides to a great extent. Firstly, the presence of highly negatively charged polyelectrolytes in the biofilm matrix offers diffusion resistance to antimicrobials protecting the biofilm against chemical stresses (Nichols *et al.* 1988). Secondly, the viscoelastic properties, as a result of the structural composition, dictate the ability of biofilms to deform and adapt under mechanical stresses, thereby influencing its removal (Stewart & Franklin 2008, Körstgens *et al.* 2001, Klapper *et al.* 2002, Peterson *et al.* 2015). Therefore, investigating the biofilm structure itself and its response to various stresses is important (Xiao *et al.* 2012, Koo *et al.* 2013).

In general, the antibiofilm effect of biocides has been tested mostly on biofilms of known bacterial composition but unknown structural organization. Moreover, Confocal laser scanning microscopy (CLSM) is most often used to evaluate the outcome of a chemical treatment against biofilms, focusing mainly on bacterial killing and not biofilm removal. In addition, although CLSM also provides information on the amount and spatial distribution of labelled biofilm components, it constitutes an inherently flawed method with known limitations (Azeredo *et al.* 2017). Hence, more techniques are needed, preferably applied in tandem and in a supplementary fashion in order to study the post-treatment fate of the biofilm structure.

Low load compression testing (LLCT) is a method used to study the viscoelastic behaviour of biofilms. It records the stress relaxation that occurs while the biofilm is being compressed axially with a given load and for a given time (Peterson *et al.* 2013). The stress relaxation data can be mathematically fitted using a generalized Maxwell model (Fig. 1), in which each element has a spring constant related to the elastic part of the biofilm and a characteristic decay time constant related to the ratio of the viscous and elastic parts. Three elements have been described, namely, the fastest relaxation element attributed to water flow in the biofilm under mechanical stress (lowest viscosity), the slowest element to the bacterial cells (highest viscosity) and the intermediate element to EPS/eDNA constituents (Peterson *et al.* 2013). Recently, an association between biofilm structure and penetration of disinfectants was demonstrated using LLCT (He *et al.* 2013), thereby expanding our understanding on the utility of this method for studying the post-treatment chemically affected biofilm structure.

Optical coherence tomography (OCT) is a 'non-invasive' imaging method enabling multiple assessments on the same biofilm samples, biofilm height determination and illustration of the biofilm structure (Wagner & Horn 2017). Optical coherence tomography yields greyscale images representing a sagittal cross-section of a biofilm sample. Data acquisition is based on low-coherence interferometry. Light

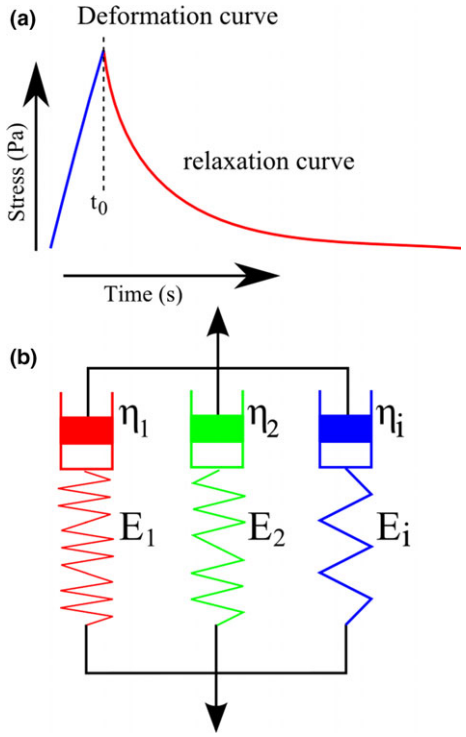

Figure 1 Representation of viscoelastic model for biofilms (modified from He *et al.* 2013). (a) Deformation curve consisting of applied stress (Pa) until t_0 and relaxation over time (s). (b) Schematic presentation of the generalized Maxwell model, comprised of spring constant E_i, viscosity η_i.

scattering is measured and due to the proportional relation between reduction in light penetration and biofilm density and thickness (Lambert-Beer Law), the generation of layers of different greyscale density within the biofilm is attainable. By analysing the shifting that occurs at the greyscale level after the application of a biocide, biofilm structure alterations can be visualized and measured.

Oral biofilms exhibit various structural arrangements and *in vitro* biofilms cultured under different conditions share many structural similarities with these *in vivo* oral biofilms (He *et al.* 2013). In the present study, two endodontically relevant bacterial species were used. *Streptococcus oralis* is a facultative anaerobe Gram-positive species and *A. naeslundii* is a strict anaerobe Gram-positive species. Both are resistant to root canal disinfection procedures and therefore frequently encountered as root canal 'persisters' (Chávez de Paz *et al.* 2003). Additionally, their capacity to coaggregate and form robust biofilms with viscoelastic properties comparable to *in vivo* oral biofilms has been established previously (Palmer *et al.* 2003, He *et al.* 2013). The two bacterial species were cocultured under specific conditions, in order to grow standardized multispecies biofilms exhibiting different structural architecture (water, EPS and bacterial density). After validating the differences in the structure of the cultured biofilms with the aid of LLCT and CLSM, the influence of the biofilm structure itself on the chemical removal capacity of 2% sodium hypochlorite (NaOCl), 17% ethylene-diamine-tetra-acetic acid (EDTA) and 2% chlorhexidine (CHX) were investigated with OCT. In addition, analysis of the post-treatment remaining biofilms was performed. For that purpose, CLSM was used to detect changes occurring on the bacterial and EPS components of each distinct biofilm structure after treatment and LLCT to evaluate irrigant-induced alterations on specific viscoelastic elements of the different biofilms.

Materials and methods

Bacterial strains and growth conditions

The clinical isolates *S. oralis* J22 and *A. naeslundii* T14V-J1 were grown as described previously (He *et al.* 2013). Briefly, the bacteria were streaked on blood agar plates and a single colony was used to inoculate 10 mL modified brain heart infusion broth (BHI) (37.0 g L^{-1} BHI, 1.0 g L^{-1} yeast extract, 0.02 g L^{-1} NaOH, 0.001 g L^{-1} Vitamin K1, 5 mg L^{-1} L-cysteine-HCl, pH 7.3) (BHI, Oxoid Ltd., Basingstoke, UK). Subsequently, *S. oralis* were cultured at 37 °C for 24 h in ambient air and *A. naeslundii* at 37 °C for 48 h in an anaerobic chamber (pre-cultures). Pre-cultures were used to inoculate 50 mL modified BHI (1:20 dilution) and grown for 16 h (main cultures). Bacteria were harvested by centrifugal force (6350 g) and washed twice in sterile adhesion buffer (0.147 g L^{-1} $CaCl_2$, 0.174 g L^{-1} K_2HPO_4, 0.136 g L^{-1} KH_2PO_4, 3.728 g L^{-1} KCl, pH 6.8). The bacterial pellets were suspended in 10 mL sterile adhesion buffer and sonicated intermittently in ice-water for 3 × 10 s at 30 W (Vibra cell model 375, Sonics and Materials Inc., Newtown, CT, USA) to break bacterial chains. Bacteria were counted in a Bürker-Türk counting chamber (Marienfeld-Superior, Lauda-Königshofen, Germany) and both suspensions were diluted in adhesion buffer in order to prepare a dual-species bacterial suspension of a concentration of 6×10^8 bacteria/mL for *S. oralis* and 2×10^8 bacteria/mL for *A. naeslundii*.

Biofilm growth

In order to obtain biofilms with different structures, and therefore mimic the structural variety of biofilms found in the oral cavity, several growth conditions were applied. Specifically, the constant depth film fermenter (CDFF) was used for the growth of steady-state biofilms. This was achieved through the repeated cycles of scraping/compaction and the limited dropwise supply of nutrients that takes place during biofilm formation in this apparatus, eventually leading to dental plaque-like bacterial dense biofilms (Kinniment *et al.* 1996, Rózenbaum *et al.* 2017). Briefly, the CDFF was equipped with 15 sample holders and each holder included five saliva-coated hydroxyapatite (HA) discs of 5 mm diameter each that served as the substrate for biofilm growth. For the saliva coating, freeze-dried whole saliva pooled from at least 20 healthy volunteers of both genders (saliva collection was performed in agreement with the guidelines set out by the Medical Ethical Committee at the University Medical Center Groningen, Groningen, The Netherlands, approval letter 06-02-2009) was dissolved in 30 mL adhesion buffer (1.5 g L^{-1}), stirred for 2 h and centrifuged at 15 000 g, 10 °C for 5 min. The HA discs were exposed to the reconstituted saliva for 14 h, at 4 °C, under static conditions. The saliva-coated HA discs were placed on the stage platform of the holders, which were already recessed to a depth of 250 μm in order to allow for the growth of biofilms of standardized thickness. Following, 100 mL of the dual-species bacterial suspension was introduced dropwise in the CDFF over 1 h, while the CDFF table with the holders was kept in constant slow rotation. Subsequently, the rotation was stopped for 30 min to allow for the bacteria to adhere to the saliva-coated HA substrate. Finally, rotation was resumed and the biofilms were grown for 96 h at 37 °C under continuous supply of modified BHI with a rate of 45 mL h^{-1}.

To obtain biofilms of similar form but different structure, samples were grown in confined spaces, under static conditions and in abundance of media, but for two different time periods. Five sterile saliva-coated HA discs (diameter = 5 mm) were placed on the stage platform of the CDFF holders. The stage platforms were recessed to the maximum depth allowed by the holders (h = 2 mm), thus enabling the growth of biofilms within this confined space of the CDFF holders (maximum volume for biofilm growth = πr^2 h = 3.14 × $(2.5\ mm)^2$ × 2 mm = 39.3 mm^3). The HA disc-carrying CDFF holders were immersed in a volumetric jar with 20 mL of the dual-species bacteria suspension and left undisturbed for 30 min to allow for bacterial adhesion to occur. The bacterial suspension was subsequently decanted and 20 mL of modified BHI was added and refreshed every 24 h for 4 and 10 days.

Application of the endodontic irrigants

Twenty samples of each type of biofilm were used, divided into four groups according to the endodontic irrigant applied. Biofilms were treated with adhesion buffer, 2% NaOCl, 17% EDTA and 2% CHX, all in liquid form, by applying once statically (no flow) 20 μL solution over the biofilms and leaving the samples undisturbed for 60 s. Subsequently, adhesion buffer was gently pipetted over the biofilms to neutralize EDTA and CHX, while NaOCl solution was neutralised by gently pipetting 4.23% sodium thiosulfate ($Na_2S_2O_3$, Sigma-Aldrich, St Louis, MO, USA).

Optical coherence tomography (OCT) and biofilm removal assessment

Biofilm removal quantification was carried out with the OCT by comparing pre- and post-treatment acquired images. During OCT imaging, the biofilms were kept in a volumetric jar with adhesion buffer. Real-time 2D cross-sections representative for the biofilm were acquired with an OCT scanner (Thorlabs, Newton, NJ, USA). The field of view was set up to 45 mm, the refraction index to 1.33 and images were processed with the ThorImage OCT software (Thorlabs). To increase the reproducibility of the image analysis, Fiji (open source software) was used to calculate the distance in every column of pixels between the substrate and top of the biofilm (4500 rows of pixels). To improve the accuracy of the data, different thresholds in one image were selected (Otsu 1979, Liao *et al.* 2001). This resulted in the identification of several layers in the biofilm. The results of the experiments showed that the layer exhibiting the lower greyscale pixel intensity was easily detached from the underlying biofilm just by passing the biofilm through an air-liquid interface; this was assigned to the term '*disrupted layer*'. The layer with the higher greyscale pixel intensity could remain relatively undisturbed and attached to the substrate; this was assigned to the term '*coherent layer*' (Fig. 2). Percentage biofilm reduction was the outcome measure. This was calculated from the OCT pre- and post- treatment measurements of the coherent layer for every treatment. Biofilm behaviour during

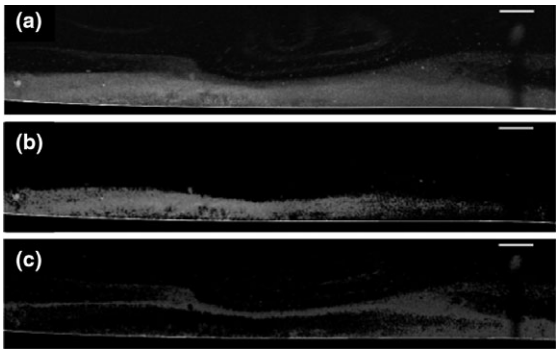

Figure 2 Multilevel greyscale thresholding from representative NaOCl-treated constant depth film fermenter biofilm. Identification of different biofilm layers imaged with the optical coherence tomography (OCT). The degree of coherence of each layer was correlated to its corresponding greyscale level. (a) Original image of biofilm acquired with OCT, split after multilevel thresholding in (b) Coherent layer (higher greyscale level pixel intensity) and (c) Disrupted layer (lower greyscale level pixel intensity) (scale bar: 250 μm).

contact with the endodontic irrigants was also registered 'real-time' by recording OCT videos (FOV size of 45 mm and refraction index of 1.33, frame rate: 0.4 image/s). Biofilms were placed in a parallel plate flow chamber and endodontic irrigants were introduced with low flow rate (approximately 2.5 mL min^{-1}). The effects induced by the irrigants were recorded during a 5-min time lapse.

Low load compression testing (LLCT) and assessment of biofilm viscoelastic properties

Biofilms were compressed to a 20% deformation within 1 s, after which the deformation was held constant for 100 s (He *et al.* 2013). The relaxation was monitored over time and normalized over the cross-sectional area of the plunger to calculate the induced stress (Fig. 1a). The percentage change in induced stress occurring within 100 s from its initial value was termed the percentage stress relaxation (R). The stress relaxation curves for each biofilm were modelled using a generalized Maxwell model, by fitting experimentally measured data to Equation (1). A generalized Maxwell model is composed of a number of Maxwell elements connected in parallel (Fig. 1b). Each Maxwell element is in turn composed of a spring (representing the elastic property) and a dash-pot (representing viscous property) in series to be able to quantify the viscoelasticity. Each Maxwell element is characterized by the spring constant (E) and the relaxation time constant (τ). In Equation (1), E(t) represents the total stress exerted by the biofilm divided by the imposed strain. The relative importance of each element (RI) was expressed as the percentage of its spring constant to the sum of the spring constants of all elements at $t = 0$ using Equation (2). Samples were submerged in adhesion buffer during measurements and due to the sensitivity of the weigh and to the duration of the measurements (100 s), a correction for water evaporation was applied.

$$E(t) = E_1 e^{t/\tau_1} + E_2 e^{t/\tau_2} + E_3 e^{t/\tau_3} + E_4 e^{t/\tau_4} \quad (1)$$

$$\mathrm{RI}_i = E_i/(E_1 + E_2 + E_3 + E_4) \quad (2)$$

where i varies from 1 to 4.

Confocal laser scanning microscopy (CLSM) and visualization of biofilm composition

Biofilms were stained with live/dead stain (BacLight™, Invitrogen, Breda, The Netherlands) (1:3 ratio) for 20 min and with calcofluor white to stain the EPS (polysaccharides) (20 μL mL^{-1}, 3.8 mmol L^{-1}) for 10 min. Following, they were submerged in 15 mL adhesion buffer and kept protected from light until imaging. A CLSM (Leica TCSSP2, Leica Microsystems GmbH, Heidelberg, Germany) was used to record a stack of images from two different randomly selected locations on each biofilm with an 8 × 40 water objective lens, with 1024 × 1024 pixels. The ratio of red (disturbed bacterial cell wall integrity), green (intact bacterial cell wall) and blue (EPS) to the overall volume of the biomass were calculated with COMSTAT software (Heydorn *et al.* 2000). Due to the inherent limitations of the technique regarding dye penetration (approximately 60 μm staining penetration depth), only the top layer of the biofilms was evaluated.

Statistical analysis

Statistical analysis was performed using SPSS software (Version 23.0, IBM Corp., Armonk, New York, USA). For analysis of the OCT data a two-way analysis of variance (ANOVA) was carried out, with biofilm type (three levels) and irrigant treatment (four levels) being the two independent variables. Tukey HSD *post hoc* was performed for the analysis of the main effect of each independent variable on biofilm reduction (outcome measure) and further analysis of the interaction between the two independent variables was

carried out through simple effect analysis. LLCT and CLSM data for the post-treated remaining biofilms were analysed through one-way ANOVA and Dunnett's *post hoc* test; within each biofilm type, multiple comparisons between the different irrigant treatments and the buffer treatment (control) were made. The level of statistical significance was set at $a < 0.05$. Pearson's r correlation coefficient was computed to assess the association between the stress relaxation (R) and the unique spring constants ($E_{1–4}$) as well as the relationship between the biofilm viscoelastic elements (LLCT) and the biofilm composition (CLSM).

Results

The following abbreviations are used to describe the different types of biofilms in this study:

4CDFFB: 4-day CDFF grown biofilm, **4SB**: 4-day statically grown biofilm, **10SB**: 10-day statically grown biofilm.

Viscoelastic elements associated with biofilm structural components

LLCT analysis from all samples yielded four unique decay times (τ_i, s), that based on the frequency were binned to the following time intervals: τ_1: 0.01–<0.5 s, τ_2: 0.5–<3 s, τ_3: 3–<100 s, and τ_4: >100 s (Fig. 3). Allocating these decay times to spring constants during the stress relaxation data fitting analysis resulted in four spring constants or components, namely E_1, E_2, E_3 and E_4. Based on the hydrogel model (Pasqui *et al.* 2012) and on previous publications (Peterson *et al.* 2013, He *et al.* 2013), E_1 was ascribed to 'free water', E_2 to 'bound water', E_3 to EPS-related material and E_4 to bacterial cells. Additional analysis yielded a strong negative correlation between stress relaxation (R) and E_4 (Pearson's $r = -0.962$, $P < 0.001$), namely the higher the E_4 the lower the R. Furthermore, R was positively correlated to E_1 (Pearson's $r = 0.767$, $P < 0.001$) and E_2 (Pearson's $r = 0.545$, $P < 0.001$). Indeed, when E_1 and E_2 were combined, a very strong correlation with R emerged (Pearson's $r = 0.927$, $P < 0.001$).

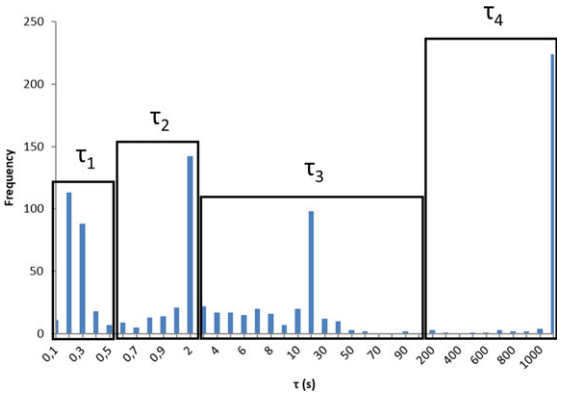

Figure 3 Frequency plot for all measured characteristic decay times (τ_i) yielded from the low load compression testing. The plot shows the τ_i distribution and the identification of the four different groups (τ_1: 0.01 < 0.5 s, τ_2: 0.5 < 3 s, τ_3: 3 < 100 s, and τ_4: >100 s).

Validation of differences in biofilm structure through LLCT and CLSM of untreated biofilms

To validate differences in the structure of the differently grown biofilms, data from untreated biofilms (no irrigant applied) were included in the analysis.

LLCT data revealed that stress relaxation was significantly lower in 4CDFFB compared to 4SB ($P = 0.002$) and 10SB ($P = 0.042$). The relative importance of the influence of the free water (E_1) was significantly higher in 4SB compared to 4CDFFB ($P = 0.005$) and 10SB ($P < 0.001$). On the other hand, the relative importance of the influence of the bacterial cells (E_4) was significantly higher in 4CDFFB compared to 4SB ($P = 0.002$) and 10SB ($P = 0.044$). The relative importance of the influence of bound water (E_2) was significantly higher in the 10SB compared to 4CDFFB ($P = 0.008$). Accordingly, the EPS-related material (E_3) was significantly higher in the 10SB compared to the 4CDFFB ($P = 0.04$) and considerably higher compared to the 4SB (Fig. 4a).

Structural differences were also confirmed by CLSM, where more dead cells and less EPS were found for 4CDFFB compared to 4SB ($P = 0.001$ for % DEAD and $P = 0.002$ for % EPS) and 10SB ($P = 0.007$ for % DEAD and $P = 0.004$ for %EPS; Fig. 4b). Figures 4c–e show representative CLSM images and OCT scans from the different types of grown biofilms.

Biofilm removal depends upon biofilm structure and type of irrigant

The main effect of biofilm structure on biofilm removal was statistically significant ($P = 0.005$). Without taking into consideration the irrigant factor, the 4CDFFB was significantly less removed compared to both statically grown biofilms ($P \leq 0.01$), whereas no differences between the 4SB and 10SB were detected (Fig. 5a). The main effect of irrigant treatment on biofilm

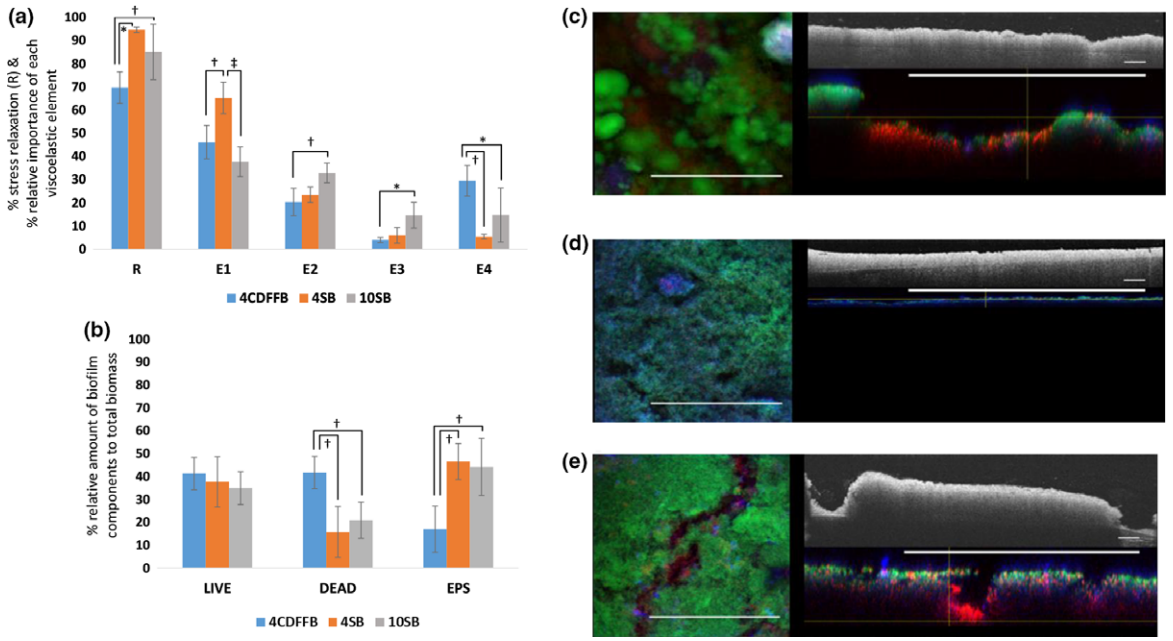

Figure 4 Validation of structural differences in untreated biofilms grown under different conditions. (a) Stress relaxation and Maxwell element analysis. (b) Relative quantification (to the total biomass) of the stained bacterial and EPS biofilm components. Values are presented as mean ± 95% confidence interval. Statistical significance is represented by * for $P \leq 0.05$, † for $P \leq 0.01$ and ‡ for $P \leq 0.001$. (c-e) Representative images of biofilms imaged by Confocal laser scanning microscopy (left panel: overview, right panel-bottom: cross-section) and optical coherence tomography (right panel-upper), (c) constant depth film fermenter (CDFF) biofilm, where areas with dense bacterial aggregations are evident, as well as extensive superficial areas with red stained bacteria (dead) due to the continuous scraping/compaction occurring during biofilm formation, (d) 4-day static biofilm, with increased presence of EPS and (e) 10-day static biofilm, where the increased thickness and density of the different stained biofilm components are evident, as well as the biofilm stratification with a dense aggregation of red stained (dead) bacterial cells internally and the green stained (live) cells externally. Scale bar represents 250 μm. 4CDFFB, 4-day CDFF biofilm; 4SB, 4-day static biofilm; 10SB, 10-day static biofilm.

removal was statistically significant ($P = 0.004$). Without taking into consideration the biofilm structure factor, NaOCl removed significantly more biofilm compared to the buffer control ($P < 0.001$) and the CHX ($P = 0.005$) and considerably more compared to the EDTA (Fig. 5b). No significant differences were detected among the other irrigants.

Biofilm structure dictates the chemical antibiofilm capacity of NaOCl

A significant interaction was detected between the biofilm structure and irrigant treatment ($P = 0.001$). Therefore, the differences in biofilm removal induced by each irrigant were viewed in relation to the different biofilm structures (simple effect analysis; Fig. 5c). Analysis of the effect of the biofilm structure within each irrigant treatment group revealed that NaOCl removed significantly less biofilm in the 4CDFFB compared to the pronounced removal observed in the statically grown biofilms ($P < 0.001$). No differences were detected between the 4SB and 10SB. Within the CHX and EDTA irrigant groups, a similar biofilm removal was recorded irrespective of the biofilm structure, with EDTA removing noticeably more biofilm in the 4CDFFB. Also, biofilm removal by control treatment (buffer) was significantly more pronounced in 4SB compared to the 4CDFFB ($P = 0.022$; Fig. 5).

Biofilm removal caused by irrigants: NaOCl affects statically grown biofilms but not the bacterial dense biofilms and CHX shows inferior biofilm removal

The differences in biofilm removal in each biofilm structure were also viewed in relation to the applied irrigant (Fig. 5c). Both within the 4SB and 10SB groups, NaOCl removed significantly more biofilm compared to all other irrigants [(4SB: $P = 0.015$

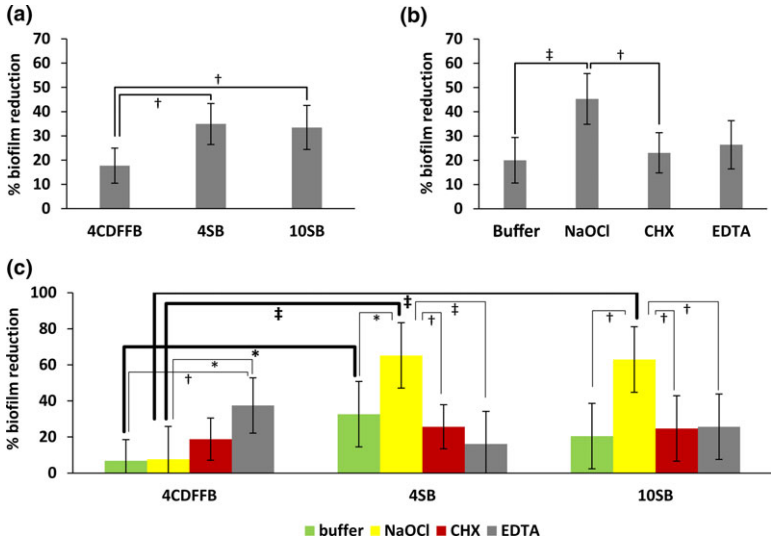

Figure 5 Two-way analysis of variance for the structure- and irrigant- dependent percentage biofilm reduction showing that biofilm reduction is influenced both by the biofilm structure and the irrigant treatment. Main effects of (a) biofilm structure and (b) irrigant treatment, on biofilm reduction. (c) Analysis of the effect of the interaction between biofilm structure and irrigant treatment on percentage biofilm reduction. Percentage biofilm reduction was compared across all levels of the two independent variables (biofilm structure, irrigant treatment). Values are presented as mean ± 95% confidence interval. The thick horizontal black lines denote statistically significant differences in % biofilm reduction among the differently grown biofilms within each irrigant treatment. The thin horizontal black lines denote statistically significant differences in % biofilm reduction among the different irrigant treatments within each biofilm structure. Statistical significance is represented by * for $P \leq 0.05$, † for $P \leq 0.01$ and ‡ for $P \leq 0.001$. 4CDFFB, 4-day constant depth film fermenter biofilm; 4SB, 4-day static biofilm; 10SB, 10-day static biofilm.

compared to buffer, $P = 0.001$ compared to CHX, $P < 0.001$ compared to EDTA) and (10SB: $P = 0.002$ compared to buffer, $P = 0.005$ compared to CHX, $P = 0.006$ compared to EDTA)]. However, in the 4CDFFB, NaOCl was significantly less effective compared to EDTA ($P = 0.017$) and EDTA was significantly more effective compared to the buffer ($P = 0.003$). The CHX-induced biofilm removal was either unremarkable compared to the other irrigants in the 4CDFFB or significantly less compared to NaOCl in the statically grown biofilms ($P = 0.001$ within 4SB and $P = 0.005$ within 10SB; Fig. 5).

Indeed, OCT 'real-time' video showed that no biofilm removal was taking place during CHX application, but rather a rearrangement of the biofilm structure was occurring (video S1).

Viscoelasticity and architecture of irrigated biofilms: biofilm age-dependent changes of viscoelastic elements after NaOCl application and CHX-induced rearrangement of biofilm structure

NaOCl treatment affected differently the biofilm types with regard to their viscoelastic properties, compared to the control biofilms (buffer treatment). In the younger biofilms (4CDFFB, 4SB), stress relaxation (R), and the relative influence of free water (E_1) were significantly reduced [(4CDFFB: $P = 0.004$ for R, $P = 0.011$ for E_1), (4SB: $P = 0.002$ for R, $P = 0.005$ for E_1)], whereas the relative influence of bacterial cells (E_4) was significantly increased [(4CDFFB: $P = 0.005$), (4SB: $P = 0.003$)]. The opposite was observed in the more mature biofilm (10SB), with E_1 showing significant increase ($P = 0.009$) and E_4 considerable decrease (Fig. 6a). In line with the latter, NaOCl exerted a significant effect on bacterial viability only in the 10SB, where a significant decrease in viable cells ($P = 0.037$) combined with an unremarkable change in dead cells was noted (Fig. 6b,c). CHX-treated CDFF biofilms showed a marked increase in the influence of the E_3 viscoelastic component, as well as a significant increase in the EPS of the top layer ($P = 0.01$; Fig. 6b,d). Furthermore, EDTA led to a significantly increased presence of dead cells in 4SB ($P = 0.003$), in combination with a significantly decreased presence of EPS ($P = 0.008$; Fig. 6b,e). However, this did not yield significant changes in the overall viscoelasticity of this type biofilm. Notably,

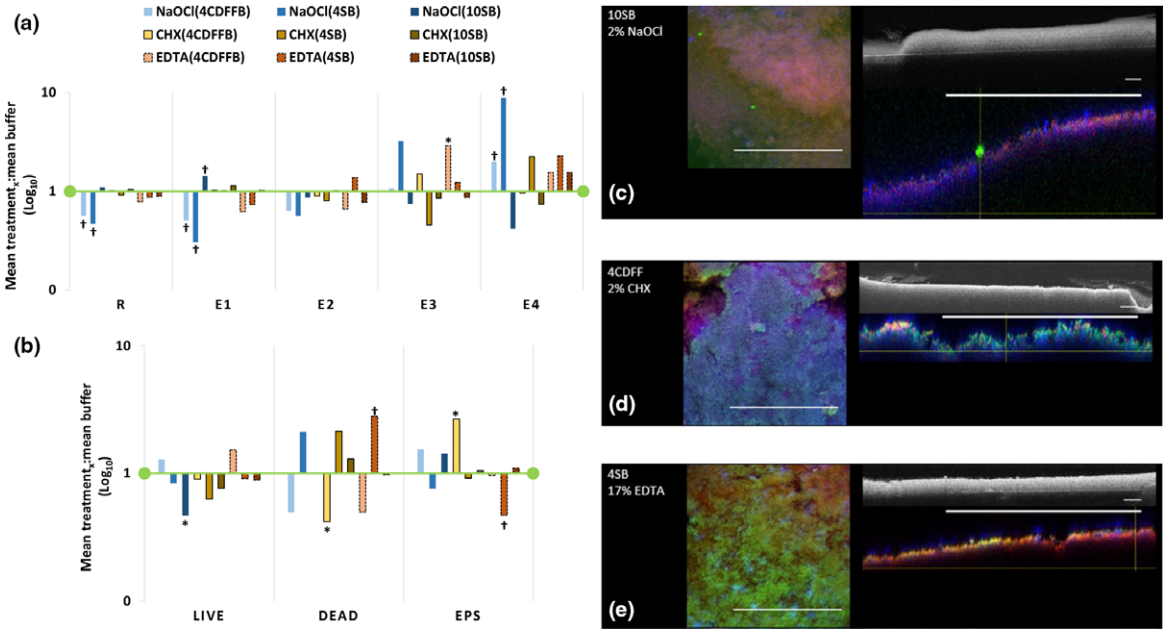

Figure 6 Semi-log plot of (a) the relative magnitude of change in the stress relaxation and the viscoelastic elements of the remaining biofilms and (b) the relative magnitude of change in the live/dead bacteria and EPS of the remaining biofilms, occurring after application of the endodontic irrigants and after adjusting for the buffer-induced changes (control group, represented by the green horizontal line in the bar graphs). Statistical significance is represented by * for $P \leq 0.05$ and † for $P \leq 0.01$. (c-e) Representative images of biofilms imaged by Confocal laser scanning microscopy (left panel: overview, right panel-bottom: cross-section) and optical coherence tomography (right panel-upper), (c) 10-day static biofilm after NaOCl treatment, where the absence of green staining denotes the removal of bacterial cells with an intact bacterial wall (live), (d) constant depth film fermenter (CDFF) biofilm after CHX treatment, where the blue staining (EPS) predominates and (e) 4-day static biofilm after Ethylene-diamine-tetra-acetic acid treatment, where the increased presence of red staining denotes the strong presence of bacterial cells with disrupted bacterial wall (dead) and the decreased presence of the blue staining the significant removal of EPS. Scale bar represents 250 μm. 4CDFFB, 4-day CDFF biofilm; 4SB, 4-day static biofilm; 10SB, 10-day static biofilm.

EDTA increased significantly the contribution of the E_3 component (EPS) on the overall viscoelastic behaviour of the bacterial dense biofilm (4CDFFB) ($P = 0.02$; Fig. 6a).

Correlations between biofilm composition and viscoelastic elements

Finally, CLSM and LLCT data from all types of biofilms and irrigant treatments were pooled and submitted to Pearson's correlation coefficient test statistics. The following significant general correlations emerged:

- % LIVE bacteria showed a significant positive correlation with E_4 ($r = 0.323$, $P = 0.01$),
- % DEAD bacteria showed no significant correlation with any of the components,
- % EPS showed a significant negative correlation with E_4 ($r = -0.323$, $P = 0.01$).

Discussion

This is the first time that the efficacy of various endodontic irrigants on removing biofilm has been shown to affect biofilm in a structure-dependent fashion. Bacterial dense biofilms, with lower water and EPS content were not removed effectively by a potent biocide, such as NaOCl, but had increased susceptibility to a chelating solution, such as EDTA. On the other hand, biofilms richer in water and EPS were more prone to NaOCl removal. A secondary finding was that CHX did not induce considerable biofilm reduction, but rather caused a rearrangement of the biofilm structure. Furthermore, the age of the biofilm influenced the viscoelastic behaviour of the remaining biofilms after the 'one-off' chemical attack with the irrigants and NaOCl changed significantly the viscoelastic pattern of younger biofilms.

Using LLCT and CLSM, differences in the architecture were demonstrated between the CDFF biofilms (high bacterial density and lower EPS content) and the statically grown biofilms (rich in bound water and EPS). These observations are also in accordance with the mode of biofilm growth in the CDFF apparatus. The continuous compaction by the polytetrafluoroethylene (Teflon) scrapers can account for the dense bacterial cell arrangement within the biofilm as well as for the increased percentage of dead cells in the upper biofilm layer (Hope & Wilson 2006, He *et al.* 2013). Moreover, in the aged statically grown biofilms, the influence of E_2 and E_3 components were significantly higher than in the younger static biofilms. This indicated both the presence of more viscous water molecules bound to the EPS structure as well as more viscous EPS material. Indeed, aged biofilms tend to have a more mature organization of their structure (Stanley & Lazazzera 2004).

Besides structural differences between differently grown biofilms, resistant spots and layer stratification within the same biofilm can be present. Indeed, regions with high bacterial density, fluffy top layers and bacterial compacted basal layers have been described (de Beer *et al.* 1994, Derlon *et al.* 2008). The biofilms used in this study were meant also to mimic the structure of multilayered biofilms possibly found in the oral environment, with the CDFF biofilms representing the basal cell dense layer or resistant spots of an oral biofilm (He *et al.* 2013) and the young static biofilms simulating the fluffier top layer.

Earlier studies on the viscoelastic behaviour of biofilms have identified three Maxwell elements. Water has been related to the fast occurring element, EPS material to the intermediate and bacterial cells to the slow appearing element (Peterson *et al.* 2013, He *et al.* 2013). This was based on the premise that water displacement (low viscosity component) and bacteria (high viscosity component) were correlated to a fast and slow reorganisation of the biofilm, respectively. Indeed, water rearrangement was associated with a decay time of $\tau < 3$ s. However, in the present study two fast elements were needed to achieve the best curve fitting during the Maxwell element analysis within this fast decay time interval, thus leading to the acknowledgement of an extra fast component. Taking into consideration the structural similarities concerning viscoelasticity between biofilms and hydrogels, it is hereby argued that biofilms could be considered as hydrogels with an extra component, that is the bacterial cells. The two fast components can be explained by different water binding possibilities in the biofilm, namely, water physically entrapped in or water bound to the EPS structure. Therefore, a new division of the fast component is suggested in line with the description of hydrogels (Pasqui *et al.* 2012):

- E_1: fast-moving water or 'free water', physically hampered by the EPS chains with no real cohesive or adhesive force,
- E_2: relatively slow moving water or 'bound water', attached to polymer chains by hydration of polar functional groups (hydrogen bonds) or ion groups (electrostriction) (cohesive or adhesive force),
- E_3: EPS-related material, namely, the bulk material surrounding the bacterial cell, excluding the water component,
- E_4: bacterial cells.

The hypothesis that E_2 represents water content of the biofilm is further supported by its positive correlation with stress relaxation. With water being a prominent component of the biofilm structure, this is expected to exert major influence on the viscoelastic behaviour of the biofilm during deformation. However, the slower decay time of the E_2 constant compared to E_1 implies that this specific water component is bound to something that results in its decelerated displacement. Accepting that water can bind to polysaccharidic chains (noncovalent interactions), it seems logical to attribute the relatively fast E_2 component to the EPS-bounded water. The strong negative correlation of E_4 to stress relaxation indicates that the presence of a dense bacterial cell component in the biofilm hinders the reorganizational flow, firstly of water and then of EPS, that normally occurs upon stress dissipation on the viscoelastic biofilm. This explains the low-stress relaxation and the decreased influence of the faster structural components (E_1, E_2 and E_3) observed in the bacterial dense CDFF biofilms in our study.

Another interesting finding was that the percentage of dead cells, or more specifically, cells with no intact cell membrane, did not seem to influence the viscoelasticity of the biofilm, as this can be inferred by the absence of any correlation of the '% DEAD' cells with the viscoelastic components. These cells probably lose their binding properties within the biofilm structure and hence, they do not contribute significantly to the biofilm viscoelastic behaviour. Only cells with an intact cell membrane show a positive correlation with the viscoelastic component E_4, supporting that E_4 is represented by the active bacterial cells in the biofilm.

A clear distinction between a disrupted and coherent layered biofilm was validated in this study.

Acknowledgement of the presence of this disrupted layer is important to clarify the effect and the mode of action of an endodontic irrigant. The disrupted layer showed a general tendency to increase after application of all applied endodontic irrigants and it was easily dissociated from the rest of the biofilm after passaging of the sample through an air-liquid interface. This reveals that a chemical effect, other than biofilm dissolution (complete removal) occurs on the biofilm. Here, it is hypothesized that the biofilm undergoes structural alterations upon static application of a chemical solution before it dissolves completely. The fate of this disrupted layer and its clinical impact are currently unknown. Nonetheless, air bubble formation caused by the air-liquid interface passaging (Gómez-Suárez *et al.* 2001), was sufficient to disrupt the retention of the disrupted layer to the underlying biofilm. Therefore, from a clinical standpoint, it stands to reason to extrapolate that cavitation induced by active ultrasonic irrigation (van der Sluis *et al.* 2007) could play a role in the removal of this loosely attached biofilm layer.

In terms of biofilm reduction, 2% NaOCl was more potent than CHX and EDTA, which is in line with findings from earlier publications (Chávez de Paz *et al.* 2010, Ordinola-Zapata *et al.* 2012, Tawakoli *et al.* 2015). Nevertheless, NaOCl had a significantly weaker effect on the bacterial dense CDFF biofilms, compared to static biofilms. This indicates that bacterial dense biofilms or biofilm layers, such as the basal layer attached to the root canal walls or the compacted biofilms present within narrow canal ramifications, might not be so receptive to the chemical effects of NaOCl. Moreover, NaOCl caused significant changes to the structure of the CDFF remaining biofilms, resulting in even stiffer biofilms, as evidenced by the significant reduction in their stress relaxation. Biofilm stiffening has been associated with compromised shear stress-induced biofilm removal (Brindle *et al.* 2011). Although this has yet to be demonstrated, this chemical 'side effect' of NaOCl application on bacterial dense biofilm could affect the additional cleaning achieved from the irrigant flow, where shear-stress forces are developed.

Chlorhexidine did not seem to exert any significant effect both in terms of biofilm removal and bacterial killing. The present study showed (i) minimal biofilm reduction in the CDFF cell-rich biofilm caused by CHX treatment, (ii) considerable increase in the influence of the E_3 component (EPS) of the post-CHX-treated CDFF biofilm and (iii) an unremarkable change in the overall viscoelastic behaviour of the post-CHX-treated CDFF biofilm. Earlier studies have reported on the refractory nature of defined biofilms to CHX (Pratten *et al.* 1998) and demonstrated that CHX is not effective in removing biofilm structure chemically (Bryce *et al.* 2009, Ordinola-Zapata *et al.* 2012). Furthermore, it has been shown that the flow of 1% CHX solution over a biofilm did not lead to chemical/mechanical biofilm removal (Rasmussen *et al.* 2016). Additionally, a decreased shear stress-induced biofilm removal has been attributed to biofilm 'stiffening' caused by CHX (Brindle *et al.* 2011) and CHX has been described in the literature as causing 'biofilm contraction' (Hope & Wilson 2004, Shen *et al.* 2016). In particular, Hope & Wilson (2004) hypothesized that biofilm contraction is related to the ionic interactions between the positively charged CHX molecules and the negatively charged extracellular polysaccharide (EPS) matrix that results in an internal collapse of the polymeric strands of the former. Alternatively, it could be also hypothesized that the structural rearrangement observed in the present study is the result of attractive forces between the EPS and the CHX, with the originally negatively charged EPS relocating upwards, attracted by and bound to the positively charged CHX.

For the first time, via OCT-captured videos, a 'structural shifting' of the biofilm during CHX application was clearly visualized. Furthermore, the significant increase in the EPS on the top layer and the increase in the influence of the E_3 component (EPS) of the CDFF cell-rich/water poor biofilms could be attributed to this 'structural shifting' of the biofilm facilitated by the typical structure of that specific biofilm type. It is highly likely that the terms 'collapse', 'stiffening' and 'contraction' used in previous studies also represent a kind of 'structural shifting' in the biofilm. This structural rearrangement is arguably inextricably linked to the type of micro-organisms and the matrix of the biofilm. In addition, the absence of any considerable decrease in biofilm height could be the result of the application time of CHX as well as the bacterial species and/or biofilm matrix composition used in the present study. However, the inferior biofilm removal capacity of the CHX, as well as the observed CHX-induced structural shift raise questions with regard to the benefits gained from the use of CHX in root canal treatment. Furthermore, the possibility of 'real-time' imaging emerges as promising tool for studying the mechanism of action of chemical solutions against biofilms. More information with regard to the biofilm

structure and viscoelastic properties is embodied in the OCT data, but further research is needed for a better understanding and interpretation of the acquired images.

Ethylene-diamine-tetra-acetic acid exhibited an increased efficacy in biomass reduction, especially in the bacterial dense CDFF biofilms. In line with the present findings, it has been demonstrated that EDTA is an effective 'antibiofilm' solution, causing biofilm dispersal (de Almeida *et al.* 2016), especially in the dense inner regions of the so-called 'mushroom-like structures' of the Gram-negative *Pseudomonas aeruginosa* (Banin *et al.* 2006). In the present study, EDTA was quite effective against bacterial dense biofilms consisting of Gram-positive bacteria. Interestingly, EDTA is known to disrupt the outer membrane of Gram-negative bacteria (Leive 1965), without exerting any direct actions on Gram-positive bacteria. The cell wall of Gram-positive bacteria presents with increased binding sites for divalent cations, such as calcium and magnesium (Thomas & Rice 2014), while these cations seem to be present in the EPS providing structural stabilization (Liu *et al.* 2017). Therefore, the presence of divalent cations acts as the intermediate 'cementing' agent between the bacteria and the EPS, hence maintaining a stable biofilm architecture. However, EDTA is a chelator, able to loosen calcium or other metal ions bound in the biofilm matrix (van der Waal & van der Sluis 2012), and thus able to affect the biofilm structure. Also, EDTA promotes biofilm detachment and can diffuse throughout the biofilm (de Almeida *et al.* 2016, van der Waal *et al.* 2017). A significant increase in the relative importance of the EPS-related material (E_3) was found after application of EDTA on the initially cell-rich but EPS-poor biofilms. This further supports the 'decementing' action of EDTA on the biofilm architecture, which results in EPS destabilization from the biofilm structure, leading thereby to the increasing influence of EPS on the viscoelastic properties that we observed. Also, in the younger EPS-rich biofilms (4SB), application of EDTA led to a decrease in the EPS and an increased bacterial cell death. Decreased EPS and reduction in viable bacteria were also shown in a study using the *P. aeruginosa* biofilm model (Liu *et al.* 2017).

This study was designed to assess the chemical efficacy of root canal irrigants against biofilms with different structure. Therefore, actions that would have resulted in mechanical biofilm disruption and/or removal of the biofilm prior to the static application of the biocides, such as mechanical instrumentation and irrigant flow, were not incorporated in this methodological protocol. This, by no means, downgrades the role of root canal instrumentation in controlling root canal infection. The mechanical action is effective in eradicating biofilms, either by removing them completely (adhesive biofilm failure) or by disrupting the biofilm architecture (cohesive biofilm failure), thus rendering the biofilm components more accessible to biocides. Arguably, it is expected that the effect of the employed biocides on previously mechanically agitated biofilms would be different in the present study, especially due to the mechanically induced disorganization of the biofilm structure. However, the root canal anatomy-driven inability of instruments to debride the entire root canal system (Peters *et al.* 2001) justifies the need for devising effective irrigation regimes against possibly intact biofilms. In that aspect, the findings of this study are relevant, providing some insights on factors (i.e. biofilm structure) that influence the chemical antibiofilm capacity of root canal irrigants.

Conclusions

The structure of a biofilm influences the chemical efficacy of endodontic irrigants. This emphasizes the need for taking this aspect into consideration, when the biofilm removal capacity of endodontic irrigants is assessed. Additionally, single outcome measures are not sufficient to monitor the complex processes taking place within the biofilm structure. Therefore, more assessment tools should be combined to reveal the full spectrum of the action of any biocide, especially in view of the many limitations associated with the CLSM. The use of CHX in root canal treatment should be revisited. On the contrary, the use of NaOCl for biofilm removal is highly encouraged, while EDTA seems to have a significant adjunctive role.

Acknowledgements

Dr. Busanello and Prof. Dr. So were financially supported by a CNPq scholarship. A part of the study was financed by a Research Grant of the European Society of Endodontology (ESE).

Conflict of interest

All other authors state explicitly that there are no conflicts of interest in connection with this article.

References

de Almeida J, Hoogenkamp M, Felippe WT, Crielaard W, van der Waal SV (2016) Effectiveness of EDTA and modified salt solution to detach and kill cells from Enterococcus faecalis biofilm. *Journal of Endodontics* **42**, 320–3.

Azeredo J, Azevedo NF, Briandet R, *et al.* (2017) Critical review on biofilm methods. *Critical Reviews in Microbiolology* **43**, 313–51.

Banin E, Brady KM, Greenberg EP (2006) Chelator-induced dispersal and killing of *Pseudomonas aeruginosa* cells in a biofilm. *Applied and Environmental Microbiology* **72**, 2064–9.

de Beer D, Srinivasan R, Stewart PS (1994) Direct measurement of chlorine penetration into biofilms during disinfection. *Applied and Environmental Microbiology* **60**, 4339–44.

Brindle ER, Miller DA, Stewart PS (2011) Hydrodynamic deformation and removal of *Staphylococcus epidermidis* biofilms treated with urea, chlorhexidine, iron chloride, or DispersinB. *Biotechnology and Bioengineering* **108**, 2968–77.

Bryce G, O'Donnell D, Ready D, Ng YL, Pratten J, Gulabivala K (2009) Contemporary root canal irrigants are able to disrupt and eradicate single- and dual-species biofilms. *Journal of Endodontics* **35**, 1243–8.

Chávez de Paz LE, Dahlén G, Molander A, Möller A, Bergenholtz G (2003) Bacteria recovered from teeth with apical periodontitis after antimicrobial endodontic treatment. *International Endodontic Journal* **36**, 500–8.

Chávez de Paz LE, Bergenholtz G, Svensäter G (2010) The effects of antimicrobials on endodontic biofilm bacteria. *Journal of Endodontics* **36**, 70–7.

Derlon N, Masse A, Escaudie R, Bernet N, Paul E (2008) Stratification in the cohesion of biofilms grown under various environmental conditions. *Water Research* **42**, 2102–10.

Flemming HC, Wingender J (2010) The biofilm matrix. *Nature Reviews Microbiology* **8**, 623–33.

Gómez-Suárez C, Busscher HJ, van der Mei HC (2001) Analysis of bacterial detachment from substratum surfaces by the passage of air-liquid interfaces. *Applied and Environmental Microbiology* **67**, 2531–7.

He Y, Peterson BW, Jongsma MA, *et al.* (2013) Stress relaxation analysis facilitates a quantitative approach towards antimicrobial penetration into biofilms. *PLoS ONE* **8**, e63750.

Heydorn A, Nielsen AT, Hentzer M, *et al.* (2000) Quantification of biofilm structures by the novel computer program COMSTAT. *Microbiology* **146**, 2395–407.

Hope CK, Wilson M (2004) Analysis of the effects of chlorhexidine on oral biofilm vitality and structure based on viability profiling and an indicator of membrane integrity. *Antimicrobial Agents and Chemotherapy* **48**, 1461–8.

Hope CK, Wilson M (2006) Biofilm structure and cell vitality in a laboratory model of subgingival plaque. *Journal of Microbiological Methods* **66**, 390–8.

Kinniment SL, Wimpenny JW, Adams D, Marsh PD (1996) Development of a steady-state oral microbial biofilm community using the constant-depth film fermenter. *Microbiology* **142**, 631–8.

Klapper I, Rupp CJ, Cargo R, Purvedorj B, Stoodley P (2002) Viscoelastic fluid description of bacterial biofilm material properties. *Biotechnology and Bioengineering* **80**, 289–96.

Koo H, Falsetta ML, Klein MI (2013) The exopolysaccharide matrix: a virulence determinant of cariogenic biofilm. *Journal of Dental Research* **92**, 1065–73.

Körstgens V, Flemming HC, Wingender J, Borchard W (2001) Uniaxial compression measurement device for investigation of the mechanical stability of biofilms. *Journal of Microbiological Methods* **46**, 9–17.

Leive L (1965) Release of lipopolysaccharide by EDTA treatment of E. coli. *Biochemical and Biophysical Research Communications* **21**, 290–6.

Liao PS, Chen TS, Chung PC (2001) A fast algorithm for multilevel thresholding. *Journal of Information Science and Engineering* **17**, 713–21.

Liu Z, Lin Y, Lu Q, *et al.* (2017) *In vitro* and *in vivo* activity of EDTA and antibacterial agents against the biofilm of mucoid *Pseudomonas aeruginosa*. *Infection* **45**, 23–31.

Nair PN (2004) Pathogenesis of apical periodontitis and the causes of endodontic failures. *Critical Reviews in Oral Biology and Medicine* **15**, 348–81.

Nair PN, Henry S, Vera J (2005) Microbial status of apical root canal system of human mandibular first molars with primary apical periodontitis after "one-visit" endodontic treatment. *Oral Surgery Oral Medicine Oral Pathology Oral Radiology and Endodontics* **99**, 231–52.

Nichols WW, Dorrington SM, Slack MPE, Walmsley HL (1988) Inhibition of tobramycin diffusion by binding to alginate. *Antimicrobial Agents and Chemotherapy* **32**, 518–23.

Ohsumi T, Takenaka S, Wakamatsu R, *et al.* (2015) Residual structure of Streptococcus mutans biofilm following complete disinfection favors secondary bacterial adhesion and biofilm re-development. *PLoS ONE* **10**, e0116647.

Ordinola-Zapata R, Bramante CM, Cavenago B, *et al.* (2012) Antimicrobial effect of endodontic solutions used as final irrigants on a dentine biofilm model. *International Endodontic Journal* **45**, 162–8.

Otsu N (1979) A threshold selection method from gray-level histograms. *IEEE Transactions on Systems, Man, and Cybernetics* **9**, 62–6.

Palmer Jr RJ, Gordon SM, Cisar JO, Kolenbrander PE (2003) Coaggregation-mediated interactions of streptococci and actinomyces detected in initial human dental plaque. *Journal of Bacteriology* **185**, 3400–9.

Pasqui D, de Cagna M, Barbucci R (2012) Polysaccharide-based hydrogels: the key role of water in affecting mechanical properties. *Polymers* **4**, 1517–34.

Peters OA, Schönenberger K, Laib A (2001) Effects of four Ni-Ti preparation techniques on root canal geometry

assessed by micro computed tomography. *International Endodontic Journal* **34**, 221–30.

Peterson BW, van der Mei HC, Sjollema J, Busscher HJ, Sharma PK (2013) A distinguishable role of EDNA in the viscoelastic relaxation of biofilms. *MBio* **4**, e00497–13.

Peterson BW, He Y, Ren Y, *et al.* (2015) Viscoelasticity of biofilms and their recalcitrance to mechanical and chemical challenges. *FEMS Microbiology Reviews* **39**, 234–45.

Pratten J, Barnett P, Wilson M (1998) Composition and susceptibility to chlorhexidine of multispecies biofilms of oral bacteria. *Applied and Environmental Microbiology* **64**, 3515–9.

Rasmussen K, Reilly C, Li Y, Jones RS (2016) Real-time imaging of anti-biofilm effects using CP-OCT. *Biotechnology and Bioengineering* **113**, 198–205.

Ricucci D, Siqueira Jr JF (2010) Biofilms and apical periodontitis: study of prevalence and association with clinical and histopathologic findings. *Journal of Endodontics* **36**, 1277–88.

Rózenbaum RT, Woudstra W, de Jong ED, van der Mei HC, Busscher HJ, Sharma P (2017) A constant depth film fermenter to grow microbial biofilms. *Protocol Exchange* https://doi.org/10.1038/protex.2017.024.

Shen Y, Zhao J, de la Fuente-Núñez C, *et al.* (2016) Experimental and theoretical investigation of multispecies oral biofilm resistance to chlorhexidine treatment. *Scientific Reports* **6**, 27537.

Siqueira Jr JF, Rôças IN (2008) Clinical implications and microbiology of bacterial persistence after treatment procedures. *Journal of Endodontics* **34**, 1291–301.

van der Sluis LW, Versluis M, Wu MK, Wesselink PR (2007) Passive ultrasonic irrigation of the root canal: a review of the literature. *International Endodontic Journal* **40**, 415–26.

Stanley NR, Lazazzera BA (2004) Environmental signals and regulatory pathways that influence biofilm formation. *Molecular Microbiology* **52**, 917–24.

Stewart PS, Franklin MJ (2008) Physiological heterogeneity in biofilms. *Nature Reviews Microbiology* **6**, 199–210.

Tawakoli PN, Ragnarsson KT, Rechenberg DK, Mohn D, Zehnder M (2015) Effects of endodontic irrigants on biofilm matrix polysaccharides. *International Endodontic Journal* **50**, 153–60.

Thomas 3rd KJ, Rice CV (2014) Revised model of calcium and magnesium binding to the bacterial cell wall. *BioMetals* **27**, 1361–70.

van der Waal SV, van der Sluis LWM (2012) Potential of calcium to scaffold an endodontic biofilm, thus protecting the micro-organisms from disinfection. *Medical Hypothesis* **79**, 1–4.

van der Waal SV, de Almeida J, Krom BP, de Soet JJ, Crielaard W (2017) Diffusion of antimicrobials in multispecies biofilms evaluated in a new biofilm model. *International Endodontic Journal* **50**, 367–76.

Wagner M, Horn H (2017) Optical coherence tomography in biofilm research: a comprehensive review. *Biotechnology and Bioengineering* **114**, 1386–402.

Xiao J, Klein MI, Falsetta ML, *et al.* (2012) The exopolysaccharide matrix modulates the interaction between 3D architecture and virulence of a mixed species oral biofilm. *PLoS Pathology* **8**, e1002623.

Supporting Information

Additional Supporting Information may be found in the online version of this article:

Video S1. Re-arrangement of the structure of a 4-day CDFF dual-species *Streptococcus oralis* J22/ *Actinomyces naeslundii* T14V-J1 biofilm after application of 2% chlorhexidine (CHX) at a flow rate 2.5 mL min^{-1} in a parallel plate flow chamber.